

Research Article

Theme: Recent Trends in the Development of Chitosan-Based Drug Delivery Systems
Guest Editors: Claudio Salomon, Francisco Goycoolea, and Bruno Moerschbacher

Development of Timolol-Loaded Galactosylated Chitosan Nanoparticles and Evaluation of Their Potential for Ocular Drug Delivery

Ruobing Zhao,¹ Jing Li,² Jingyi Wang,¹ Zhenya Yin,¹ Yongtao Zhu,¹ and Wei Liu^{1,3}

Received 29 August 2016; accepted 10 November 2016; published online 18 January 2017

Abstract. This study was conducted to develop timolol maleate (TM)-loaded galactosylated chitosan (GC) nanoparticles (NPs) (TM-GC-NPs) followed by optimization via a four-level and three-factor Box–Behnken statistical experimental design. The optimized nanoparticles showed a particle size of 213.3 ± 6.83 nm with entrapment efficiency of $38.58 \pm 1.31\%$ and drug loading of $17.72 \pm 0.28\%$. The NPs were characterized with respect to zeta potential, pH, surface morphology, and differential scanning calorimetry (DSC). The determination of the oil–water partition coefficient demonstrated that the TM-GC-NPs had a high liposolubility at pH 6 as compared to timolol-loaded chitosan nanoparticles (TM-CS-NPs) and commercial TM eye drops. The *in vitro* release study indicated that TM-GC-NPs had a sustained release effect compared with the commercial TM eye drops. Ocular tolerance was studied by the hen's egg chorioallantoic membrane (HET-CAM) assay and the formulation was non-irritant and could be used for ophthalmic drug delivery. The *in vitro* transcorneal permeation study and confocal microscopy showed enhanced penetration, and retention in the cornea was achieved with TM-GC-NPs compared with the TM-CS-NPs and TM eye drops. Preocular retention study indicated that the retention of TM-GC-NPs was significantly longer than that of TM eye drops. The *in vivo* pharmacodynamic study suggested TM-GC-NPs had a better intraocular pressure (IOP) lowering efficacy and a prolonged working time compared to commercial TM eye drops ($P \leq 0.05$). The optimized TM-GC-NPs could be prepared successfully promising their use as an ocular delivery system.

KEY WORDS: galactosylated chitosan; nanoparticle; ocular delivery; timolol.

INTRODUCTION

Glaucoma is an optic neuropathy that can gradually result in damage to the optic disc and visual field loss, usually without symptoms (1). Glaucoma is becoming a leading cause of irreversible blindness and approximately 80 million people are predicted to suffer with glaucoma by the year 2020 (2,3). Considering the major risk factor for glaucoma, the elevation of intraocular pressure (IOP) was caused by the imbalance between aqueous humor drainage and secretion and lowering IOP plays a vital role in the long-term treatment of glaucoma

(4,5). Topically applied beta-adrenergic-blocking agent timolol maleate (TM) is a common treatment for ocular hypertensive patients that decreases IOP by reducing the aqueous humor production from the ciliary body (6,7). Although timolol has been used clinically for many years, its precise mechanism for lowering aqueous humor formation is not well understood. Timolol may inhibit NaK ATPase in the ciliary epithelium (analogous to vanadate or ouabain), reduce the blood-aqueous flux of ascorbate (analogous to phlorizin), inhibit Na⁺/K⁺/Cl⁻ transport in the ciliary epithelium, or inhibit plasma flow to the ciliary processes (8).

TM eye drops are easy to instill in ocular cul de sac. However, conventional ophthalmic solutions are rapidly eliminated by blinking reflex, nasolacrimal drainage, lacrimation, and drainage by gravity, which lead to short precorneal residence and poor bioavailability (9–11). Consequently, frequent administration is required to maintain anticipated therapeutic effect. Several adverse effects such as cardiovascular, respiratory, and central nervous system toxicity (12) are caused by systemic absorption and poor patient compliance, creating substantial challenges (13).

¹ Department of Pharmaceutics, School of Pharmaceutical Science, Zhengzhou University, 100 Kexue Dadao, Zhengzhou, 450001, Henan, People's Republic of China.

² Qilu Pharmaceutical Co., Ltd., Jinan, Shandong, People's Republic of China.

³ To whom correspondence should be addressed. (e-mail: liuweiyxy@zzu.edu.cn)

Research efforts have focused on improving the retention time on the cornea and ocular bioavailability including ocular inserts, collagen shields, and *in situ* gelling systems. These administration methods are not exempt from risks, such as blurred vision, sticking of the eyelids, and low patient compliance (14). Compared with traditional eye drops, nanoparticles (NPs) have attracted considerable attention in recent years because they can protect encapsulated molecules while facilitating transport to different compartments of the eye and provide the sustained release of medication (15).

Chitosan (CS) is a cationic polymer with good potential to prolong corneal residence time of drugs owing to its interactions with the negative charged mucus and conjunctiva (15–17). Biodegradability, biocompatibility, and nontoxicity are included in favorable biological properties of CS that allow its use as a vehicle for ophthalmic formulations (18). Unfortunately, CS is only soluble in acidic solution which limits its application due to severe irritation to the eyes (19). Galactosylated chitosan (GC), a derivative of chitosan that is water soluble at neutral pH, is synthesized by covalently binding D-galactose units to CS through O-1, 6 glycosidic linkages. GC exhibits better water solubility, mucoadhesion, and cell compatibility than CS while maintaining low toxicity (20). Additionally, the pH of GC solution is closer to ocular physiological pH. The rate-limiting barrier for drug absorption is the cornea, which could be divided into main three heterogeneous layers, epithelium, stroma, and endothelium, with each layer offering a different polarity (21,22). High pH contributes to promoting unionized fraction of the drug penetration through the cornea (23). To the best of our knowledge, there have been no reports of GC used as a carrier for ophthalmic drug delivery.

The present study aims to develop a suitable and mucoadhesive nanoparticulate system consisting of TM-GC-NPs. We evaluate the potential of the developed formulation for ophthalmic drug delivery with the hope of enhanced therapeutic effects and diminished side effects.

MATERIALS AND METHODS

Materials

CS (molecular weight, 40–60 kDa; deacetylation degree, 91.3%) was purchased from the Qinghai YunZhou Biological Technology Co., LTD, China. GC (galactosylation degree, 7.1%) was synthesized at the School of Pharmaceutical Sciences, Zhengzhou University. Sodium polyphosphate (TPP) was purchased from the Tianjin Fengchuan Chemical Reagent Science and Technology Co., Ltd. TM (purity >99.9%) was purchased from the Wuhan Yuanqi Chemical Co., Ltd. TM eye drops were purchased from the Hubei Qianjiang Pharmaceutical Co., Ltd. All other chemicals and solvents used were of analytical grade, and deionized and sterilized distilled water was used in the study.

Preparation of Nanoparticles

The TM-GC-NPs were prepared by an ionic cross-linking method (24). GC and TPP were dissolved separately in deionized water until transparent solutions were obtained. TM was dissolved in the GC solution with stirring until the

mixture was homogeneous. The TPP solution was slowly added to the mixture with magnetic stirring at 30°C. The resulting TM-GC-NP suspension was kept stirring for 20 min for further crosslinking. Finally, TM-GC-NPs were collected by ultracentrifugation with a cooling centrifuge (Hitachi CP100NX, Japan) at 12,000 rpm and 4°C for 30 min and freeze-dried at –80°C for 24 h followed by lyophilization in a freeze dryer (Christ, Osterode, Germany). TM-CS-NPs were prepared by the same method using CS dissolved in acetic acid solution 0.5% (*v/v*).

Experimental Design

A four-factor, three-level factorial Box–Behnken design was employed for the optimization procedure based on the single factor designs (data not shown), using the concentration of GC (X_1) and TPP (X_2) and the mass ratio of GC/TPP (X_3) and TM/GC (X_4) as independent variables. Particle size (Y_1), encapsulation efficiency (Y_2), and loading capacity (Y_3) were taken as response for investigation. Factors and levels of the central composite design were shown in Table I. The experimental design was evaluated and optimized by Design Expert software (Design-Expert.V8.0.6.1) (25,26).

Physicochemical Characterization

Particle Size and Zeta Potential of NPs

Particle size and zeta potential of the NPs were determined by dynamic light scattering using a Malvern Zetasizer Nano ZS90 (Malvern Instruments, Worcestershire, UK). All size and zeta potential measurements were carried out at 25°C using disposable polystyrene cells and disposable plain folded capillary zeta cells, respectively. The pH values were determined at 25°C using a pH-meter (Model pH-3C Shanghai Precision & Scientific Instrument Co., Ltd, China) (27). All measurements were performed in triplicate.

Morphological Analysis of Nanoparticles

The morphological examination of the TM-GC-NPs was performed with a JEM-1010 transmission electron microscope (JEOL Japanese Electronics Company, Japan). Samples were placed on carbon-coated copper grids for viewing by transmission electron microscopy (TEM) (28).

Table I. Factors and Levels of Central Composite Design

Factors	Levels				
	–2	–1	0	+1	+2
$X_1/\text{mg mL}^{-1}$	1	1.38	1.75	2.13	2.5
$X_2/\text{mg mL}^{-1}$	0.6	0.8	1.0	1.2	1.4
$X_3/w:w$	3	3.75	4.5	5.25	6
$X_4/w:w$	0.25	0.44	0.63	0.81	1

Differential Scanning Calorimetry of Nanoparticles

Binding mechanism study of the dried samples were carried out by heating four materials (TM, GC, TM-GC-NPs, and TM-GC physical mixture) separately from 40 to 270°C at a heating rate of 10°C/min under a nitrogen environment with a DSC-60A (Shimadzu Corporation, Japan) (29).

HPLC Assay

HPLC instrument (Agilent 1100 series, Agilent Technologies, USA) was used for quantification of TM concentration *in vitro* throughout the study. Samples (20 µL) were injected to a Gemini C18 (5 µm, 250 × 4.6 mm) column (Agilent Technologies, USA), eluted with an isocratic acetonitrile/triethylamine 0.1% (v/v) in water (17/83) mobile phase, pH 3.00 adjusted with phosphoric acid at a flow rate of 1 mL/min. A wavelength of 295 nm was used to quantify TM concentration at 30°C.

Drug Entrapment Efficiency and Drug Loading Capacity Determination

The prepared nanoparticle suspension was centrifuged with a cooling centrifuge at 12,000 rpm at 4°C for 30 min. The TM concentration of supernatant was determined by HPLC after filtering through a 0.22-µm membrane to determine the free TM concentration (24). The freeze-dried TM-GC-NPs were used to determine the drug loading capacity. The drug entrapment efficiency (EE) and drug loading capacity (LD) were determined in triplicate and calculated as follows:

$$EE\% = \frac{W_{\text{total}} - W_{\text{free}}}{W_{\text{total}}} \times 100\%$$

$$LD\% = \frac{W_{\text{total}} - W_{\text{free}}}{W_{\text{NPs}}} \times 100\%$$

where W_{total} is the total amount of the TM used, W_{free} is the amount of the free TM in the supernatant, and W_{NPs} is the weight of freeze-dried NPs.

Apparent Oil–Water Partition Coefficient Determination

An appropriate amount TM, freeze-dried TM-CS-NPs and TM-GC-NPs were dissolved separately in phosphate buffers (pH 5.0, 5.8, 6.5, 7.0, 7.4, and 8.0) saturated with n-octanol and shaken continuously at 100 r/min and 34°C for 48 h to reach a distribution equilibrium. The volumes of each phase were chosen so that the TM concentration in the aqueous phase before and after distribution could be measured by the HPLC procedure. The drug concentration in the aqueous phase was measured by HPLC after centrifugation (23). The apparent oil–water partition coefficient (P) of each sample was calculated as follows:

$$P = \frac{(C_{w1} - C_{w2})}{C_{w2}}$$

where C_{w1} and C_{w2} is the drug concentration in the aqueous phase before and after equilibrium distribution, respectively.

In Vitro Release Study

The *in vitro* release was studied using a dialysis bag method (30). Briefly, 0.5 mL TM eye drops, freeze-dried TM-CS-NPs, and TM-GC-NPs (equivalent to 1.25 mg of TM) were placed in dialysis membrane bags (MWCO 8–14 kDa) which then were immersed in fresh dissolution medium (simulated artificial tears, 50 mL). The entire system was maintained at $37 \pm 0.5^\circ\text{C}$ with continuous magnetic stirring (50 rpm) (31). At predetermined time intervals, 4 mL samples were withdrawn and replaced with equal volume of fresh media to maintain the sink condition. The sample was quantitatively analyzed using a UV spectrophotometer (Shimadzu UV-2550, Japan) at 295 nm. The percentage of cumulative TM release was calculated and a graph of percent cumulative release against time was plotted. The release of TM-CS-NP and TM-GC-NP solutions was compared with that of the commercial TM eye drops.

Ocular Tolerance Test (HET-CAM Test)

The hen's egg test-chorioallantoic membrane (HET-CAM) assay was performed to assess the ocular tolerability of the developed formulation (32). Fertilized hen's eggs from a poultry farm were incubated at $37 \pm 0.5^\circ\text{C}$ and rotated manually every 12 h. Eggs were tested with a cold lamp on the ninth day to ensure that all were viable. On day 10, the egg shell was scratched off around the air cell using forceps. The inner membrane was moistened with PBS solution warmed to 37°C and carefully removed without injuring any underlying blood vessels to expose the CAM. Solutions of commercial eye drops and TM-CS-NP and TM-GC-NP solutions (0.5 mL each) were instilled directly onto the CAM surface which was then rinsed with distilled water. 0.1 M NaOH and 0.9% NaCl solution were used as positive and negative controls, respectively. Each test was performed in triplicate and the mean score of three eggs was determined. The CAM was examined for vascular damage as the sign of hyperemia, lysis, and coagulation for 5 min and then the irritation scores (IS) were calculated using the following equation:

$$IS = \frac{(301 - \text{sec}H) \times 5}{300} + \frac{(301 - \text{sec}L) \times 7}{300} + \frac{(301 - \text{sec}C) \times 9}{300}$$

where sec is the onset of reaction in seconds, H is hemorrhage, L is lysis, and C is coagulation.

The irritation classification according to the IS values was shown in Table II.

Table II. Classification of Irritation Scores for HET-CAM Assay

Irritation scores	Irritation assessment
IS < 1	Non-irritant
1 ≤ IS < 5	Mild irritant
5 ≤ IS < 10	Moderately irritant
IS ≥ 10	Severe irritant

IS irritation scores

Table III. Design Layout of Central Composite Design and Summary of Experimental Results

Run	X1 mg/ml	X2 mg/ml	X3 w:w	X4 w:w	Y1 nm	Y2%	Y3%
1	1	1	4.5	0.63	194.3	35.62	13.77
2	1.38	1.2	3.75	0.44	325.5	34.77	8.46
3	1.75	1	4.5	1	311.4	41.6	20.8
4	1.75	1	4.5	0.63	269.9	41.24	15.92
5	2.13	1.2	3.75	0.44	234.1	36.64	11.24
6	1.75	0.6	4.5	0.63	202.8	32.21	19.87
7	1.75	1	4.5	0.25	270.4	35.99	7.23
8	1.75	1	4.5	0.63	274.7	38.5	14.86
9	2.13	1.2	5.25	0.81	327.5	37.21	16.68
10	2.5	1	4.5	0.63	286.5	39.55	15.32
11	1.75	1.4	4.5	0.63	231	38.08	17.74
12	1.75	1	4.5	0.63	237	32.92	12.71
13	2.13	1.2	3.75	0.81	265.7	32.71	14.67
14	1.75	1	3	0.63	541	46.32	17.88
15	1.38	0.8	3.75	0.81	367.4	38.52	17.27
16	1.38	0.8	5.25	0.44	212.3	35.68	10.92
17	1.38	1.2	5.25	0.44	268	36.15	11.13
18	1.75	1	6	0.63	316.3	38.36	14.81
19	1.75	1	4.5	0.63	272.2	36.31	14.03
20	2.13	0.8	3.75	0.44	356.7	46.44	14.14
21	1.75	1	4.5	0.63	257.9	34.58	13.37
22	1.75	1	4.5	0.63	240.2	41.38	16.6
23	2.13	0.8	5.25	0.44	246.3	35.44	10.86
24	1.38	0.8	3.75	0.44	315.7	35.55	10.95
25	1.38	1.2	3.75	0.81	280.3	53.07	19.6
26	2.13	1.2	5.25	0.44	274.7	41.13	12.62
27	1.38	1.2	5.25	0.81	276.6	44.38	19.87
28	2.13	0.8	3.75	0.81	519.6	40.02	17.92
29	1.38	0.8	5.25	0.81	205.9	39.71	17.84
30	2.13	0.8	5.25	0.81	215.1	32.71	14.67

In Vitro Transcorneal Permeation Study

The *in vitro* transcorneal permeation study was performed on freshly excised rabbit cornea using a modified

Franz diffusion cell apparatus consisting of a donor and a receptor compartment (0.90 cm i.d., effective diffusion area of 0.70 cm², and volume of 7.8 mL). Excised rabbit cornea with a small ring of sclera tissue was mounted between the donor and receptor chamber of the modified Franz diffusion cell in a way that the epithelial surface faced the donor chamber. The receptor chamber was filled with glutathione bicarbonate ringer (GBR) buffer as diffusion medium (33). Samples of the commercial TM eye drops and TM-CS-NP and TM-GC-NP solutions (1 mL each) with concentration of 0.25% were placed into the donor compartment. The whole system was maintained at 37°C with continuous stirring. A 200 µL sample of the receptor medium was withdrawn at 15, 30, 60, 120, 180, 240, 300, and 360 min and replaced immediately with an equal volume of preheated GBR buffer. The amount of TM permeating across the cornea was quantitatively analyzed by HPLC at 295 nm (27). A graph of cumulative penetration amount per unit area against time was plotted. The corneal permeability coefficient (P_{app}) was calculated as follows:

$$P_{app} = (\Delta Q) / (\Delta t \cdot C_0 \cdot A \cdot 3600)$$

where Q indicates the cumulative penetration amount of TM permeation at time t , $\Delta Q/\Delta t$ is the linear portion of the slope, C_0 is the initial concentration of TM in the donor compartment, A is the exposed corneal surface area, and 3600 is the conversion constant from hours to seconds.

Confocal Laser Scanning Microscopy Study

Confocal laser scanning microscopy (CLSM) study was used to determine the penetration of commercial eye drops and TM-CS-NP and TM-GC-NP solutions on excise rabbit cornea by using the fluorescent reagent fluorescein isothiocyanate FITC. The permeation experiments were undertaken using NPs containing FITC prepared using the procedure described in “In Vitro Transcorneal Permeation Study” section. The cornea was removed and washed with distilled water after 1 h. The treated area was cut out,

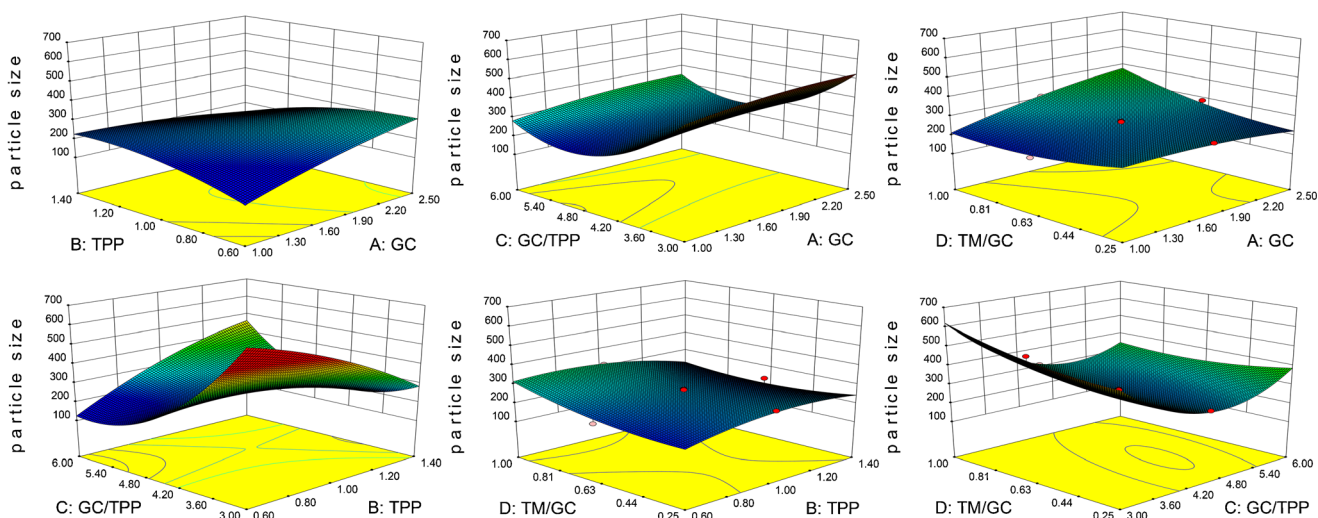


Fig. 1. 3D plots showing relative effects of different process parameters on particle size

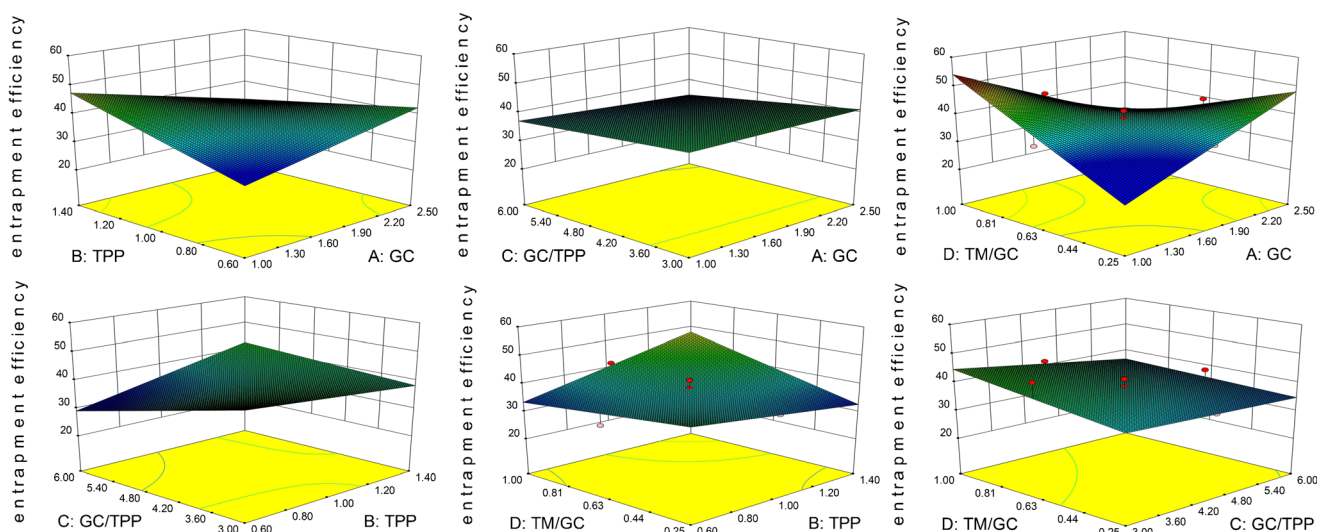


Fig. 2. 3D plots showing relative effects of different process parameters on entrapment efficiency

positioned on the microscopic slide and covered with the cover slip. Imaging was performed by a confocal laser scanning microscope (Nikon A1R/A1, Japan) with an argon laser beam with excitation at 488 nm and emission at 590 nm. The permeated depths of the formulations were detected at z -axis with NIS Elements software (29).

Preocular Retention Study

Precorneal retention time of each formulation was assessed after instillation of three formulations with/without IR 783, which included TM eye drops, TM-CS-NPs, or TM-GC-NPs, onto the left cornea of rabbits, respectively ($n=3$). The rabbits were anesthetized using chloral hydrate (injection 2.5 mL/kg) *via* the ear vein. After 0, 0.5, 1.0, 1.5, and 2.0 h, the rabbits were detected in head using the *in vivo* imaging system (Fx Pro, Kodak In-Vivo Imaging System, USA) (34).

In Vivo Pharmacodynamics Study

New Zealand albino rabbits were obtained from Yangguang Tuye Technology Co. Ltd. Jiyuan, Henan, China (License No.: SCXK (YU) 2016-0001). Animals weighing between 2.0 and 2.5 kg were selected for *in vivo* study and individually housed in an air-conditioned and light-controlled room at $25 \pm 1^\circ\text{C}$ and $70 \pm 5\%$ relative humidity. They were given a standard pellet diet and provided with water *ad libitum*. All animals were healthy and free of clinically observable ocular abnormalities. All studies were conducted in accordance with the Principles of Laboratory Animal Care (NIH Publication No. 92-93, revised in 1985) and were approved by the local ethics committees for animal experimentation.

The rabbits were first anesthetized by instilling 40 μL of 1% amethocaine hydrochloride into the subconjunctival space of the lower lid. The cornea was gently punctured near the limbus using a 31-gauge needle to decompensate the anterior chamber (35). Then, 0.1 mL of 0.3% carbomer

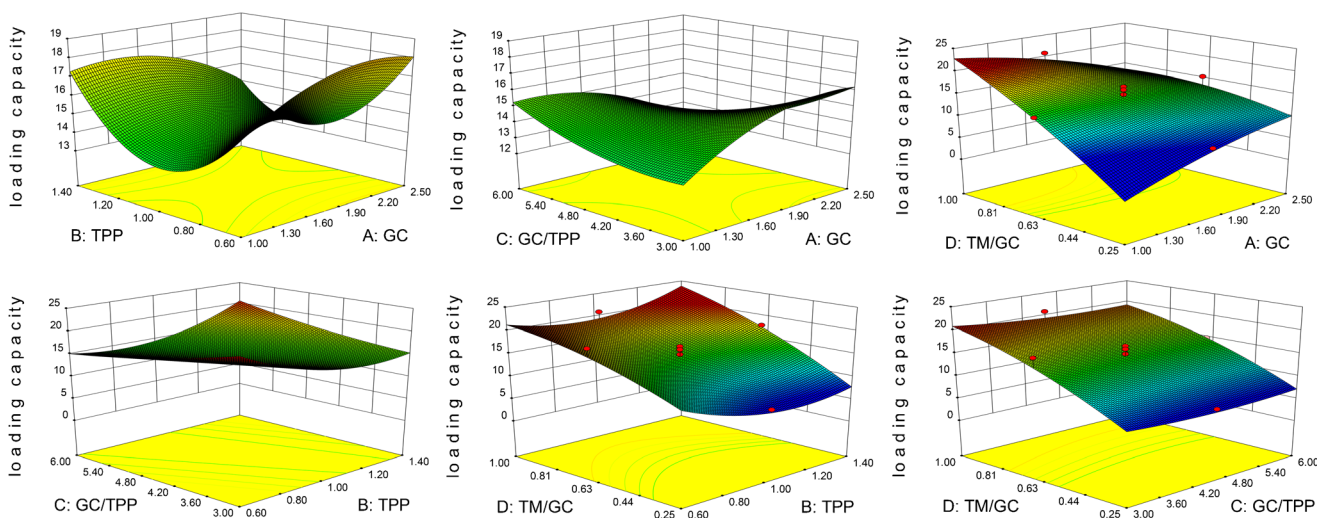


Fig. 3. 3D plots showing relative effects of different process parameters on loading capacity

solution was injected into the posterior chamber of the eye to induce ocular hypertension (35). The rabbits were considered to be glaucomatous when the IOP was higher than 21 mmHg a week after injection. The 24 rabbits were divided into four groups which were instilled 50 μ L of normal saline, 0.25% of TM eye drop, TM-CS-NP, or TM-GC-NP solutions, respectively. The normal saline group was used as the control. The intraocular pressure (IOP) was measured with a rebound tonometer (TonoVet, ICARE, Finland) at time intervals (0, 0.5, 1, 2, 4, 6, 8, 10, and 12 h) (7). Each IOP was measured three times and the mean was used for the analysis. The change in IOP (Δ IOP) was calculated as

$$\Delta \text{IOP} = \text{IOP}_{\text{control eye}} - \text{IOP}_{\text{treatment}}$$

Data Analysis

All experiments in the study were performed at least three times and the data are expressed as the mean \pm standard deviation (SD). Statistical analysis of data was performed using ANOVA.

RESULTS AND DISCUSSION

Experimental Design

Design layout of central composite design and summary of experimental results were shown in Table III.

Full quadratic polynomial equations were fitted to the data and the corresponding R^2 values were as follows.

$$Y1 = 252.04 + 15.52X1 - 5.43X2 - 45.33X3 - 17.80X1X2 + 45.06X2X3 + 43.16X3^2$$

$$(R^2 = 0.8010)$$

$$Y2 = 38.43 - 0.31X1 + 0.98X2 - 1.29X3 + 1.17X4 - 1.63X1X2 - 0.19X1X3 - 3.14X1X4 + 1.15X2X3 + 1.29X2X4 - 0.32X3X4 + 0.075X1^2 - 0.53X2^2 + 1.26X3^2 + 0.38X4^2$$

$$(R^2 = 0.6505)$$

$$Y3 = 14.55 - 0.00083X1 + 0.42X2 - 0.24X3 + 3.14X4 - 0.29X1X2 - 0.41X1X3 - 1.12X1X4 + 0.76X2X3 + 0.40X2X4 - 0.064X3X4 - 0.12X1^2 + 0.014X2^2 + 0.33X3^2 - 0.26X4^2 (R^2 = 0.8842)$$

The coefficients of determination (R^2) of obtained model were 0.8010, 0.6505, and 0.8842 for particle size, encapsulation efficiency, and drug loading, respectively. As seen, all defined

factor changes had impacts on the defined responses. Particle size was obtained in increasing order with increasing GC and TPP concentration. Same trend was also observed with variation of mass ratio of GC:TPP. The increase in GC concentration could lead to coagulation of TPP with excess cationic charge which resulted in increased particle size (36). The increase in entrapment efficiency with increase in GC concentration in GC:TPP ratio could be due to more intense ionic interaction which indicated physical entrapment of the drug in NPs. With the increase of GC concentration and mass ratio of TM:GC in a certain range, the drug loading increased.

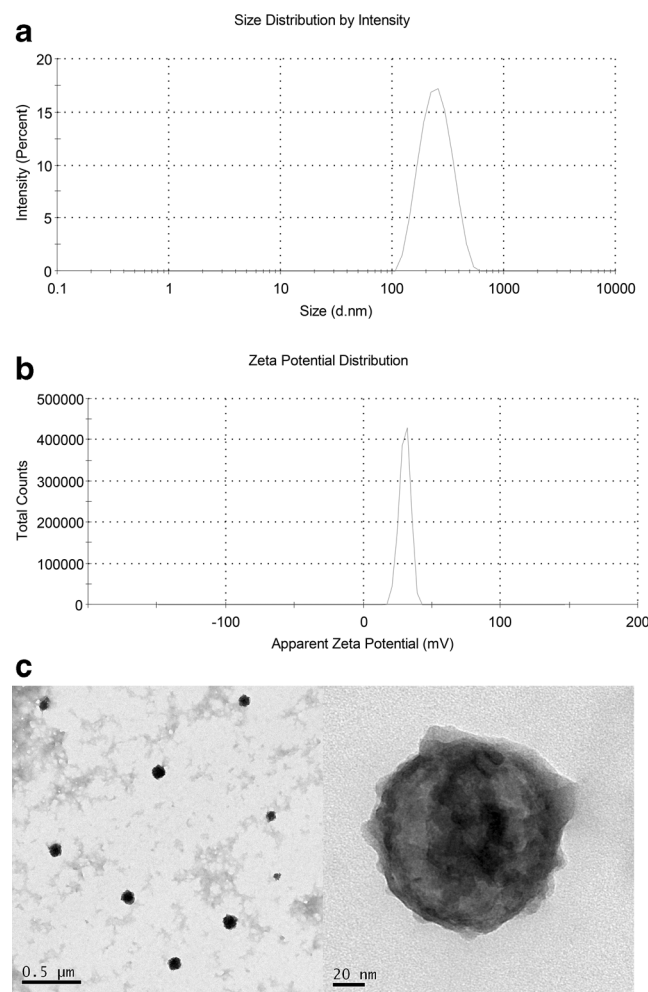


Fig. 4. TM-GC-NPs. **a** Particle size distribution. **b** Zeta potential distribution. **c** Transmission electron microscopy micrograph. **d** Images of TM-GC-NP suspension

Table IV. Predicted Values and Actual Values of Each Index Under Optimal Conditions

Response	Predicted value	Actual value	Validity (%)
Y1 (nm)	225.4 \pm 5.25	223.3 \pm 6.83	99.23
Y2 (%)	40.21 \pm 0.87	38.58 \pm 1.31	95.94
Y3 (%)	19.06 \pm 0.94	17.72 \pm 0.28	92.98

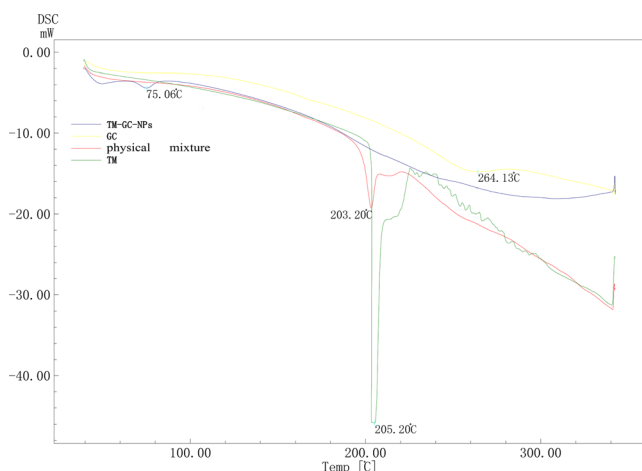


Fig. 5. DSC profiles of TM, TM-GC physical mixture, GC, and TM-GC-NPs

The effects of different factors on the particle size (Y_1), encapsulation efficiency (Y_2), and drug loading (Y_3) are represented by the three dimensional (3D) plots as shown in Figs. 1, 2, and 3.

The optimum formulations values were identified as GC (0.213% w/v), TPP (0.12% w/v), sonication time (30 min), and weight ratios of GC/TPP and TM/GC (5.25 and 0.81, respectively). These values predicted 225.4 ± 5.25 nm sized NPs, $40.21 \pm 0.87\%$ entrapment efficiency, and $19.06\% \pm 0.94$ loading capacity (Table IV). These predicted values of responses were validated by preparing NPs using the optimized process parameters and gave 223.66 ± 6.83 nm particle size, $38.58 \pm 1.31\%$ entrapment efficiency, and $17.72 \pm 0.28\%$ loading capacity. This corresponds to 99.23, 95.94, and 92.98% validity of the predicted model of predicted responses Y_1 , Y_2 , and Y_3 , respectively. This optimized formation was used for further studies.

Particle Size, Zeta Potential, pH, and Morphology of NPs

The mean diameter of the optimized NPs formulation was 223.3 ± 6.83 nm (Fig. 4a, b) and the zeta potential values was 30.2 ± 0.46 mV. The polydispersity index (PDI) was below 0.3. A particle size below 250 nm with a PDI below 0.3 was considered appropriate for ocular administration (37).

Table V. Oil–Water Partition Coefficient of TM, TM-CS-NPs, and TM-GC-NPs at Different pH

Sample	Timolol maleate		TM-CS-NPs		TM-GC-NPs	
	P	lgP	P	lgP	P	lgP
pH 5.0	0.17	-0.77	0.86	-0.06	0.99	0
pH 5.8	0.13	-0.87	0.95	-0.02	1.02	0.01
pH 6.5	0.36	-0.44	1.03	0.01	1.21	0.08
pH 7.0	0.61	-0.21	1.21	0.09	1.99	0.30
pH 7.4	1.07	0.03	2.20	0.34	3.44	0.54
pH 8.0	1.21	0.08	3.31	0.52	3.80	0.58

TM-CS-NPs timolol-loaded chitosan nanoparticles, TM-GC-NPs timolol maleate-loaded galactosylated chitosan nanoparticles

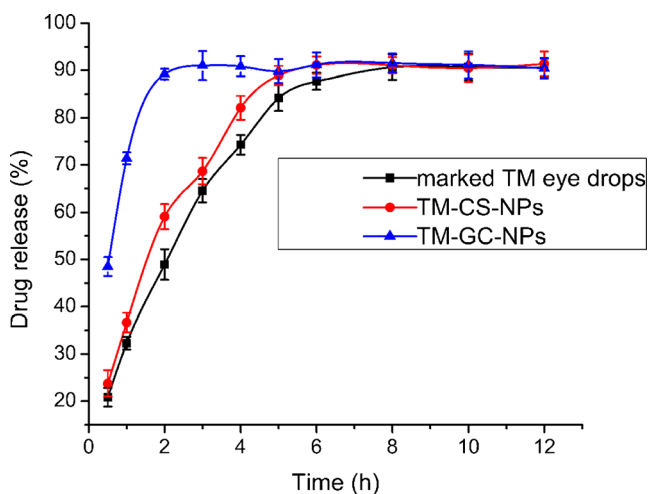


Fig. 6. *In vitro* release profiles of TM eye drops, TM-CS-NPs, and TM-GC-NPs ($n=3$, mean values \pm SD)

The pH value of commercial TM eye drops was 6.57 ± 0.12 . The pH of the TM-GC-NP and TM-CS-NP solutions was 6.05 ± 0.18 and 4.63 ± 0.23 , respectively. The pH of ophthalmic preparations should be in the range of 4 to 9 (38). The pH of TM-GC-NPs was closer to that of the commercial TM eye drops, which should decrease irritation to the eye. TEM study gave a more detailed depiction of the nanoparticles to further elucidate particle shape. The morphology of NPs showed in Fig. 4c was roughly spherical in shape. The image of TM-GC-NP suspension was shown in Fig. 4d.

Differential Scanning Calorimetry

DSC is one of the most effective approaches for studying physical interaction between drugs and the matrix of a mixture (39). The DSC thermograms of samples were presented in Fig. 5. The pure TM exhibited a sharp endotherm peak at 205.2°C . A slight shift in the position of the endothermic peak (205.2 to 203.2°C) was observed for the TM-GC physical mixture, which may be caused by solubilization of TM into the matrix and solid state interaction induced by the heating process. No TM endotherm peak was observed for TM-GC-NPs and this could be attributed to the conversion of the drug from crystalline to amorphous form after encapsulation into the polymer.

Table VI. Fit of Various Kinetic Models of TM-GC-NPs *In Vitro* Release

Model	Preparation regression equation	R^2
Zero-order	$y = 5.7598x + 38.823$	$R^2 = 0.7285$
First-order	$y = -0.2046x + 4.1836$	$R^2 = 0.8613$
Higuchi	$y = 26.837x + 12.145$	$R^2 = 0.8764$
Ritger–Peppas	$y = 33.562x^{0.4841}$	$R^2 = 0.9405$

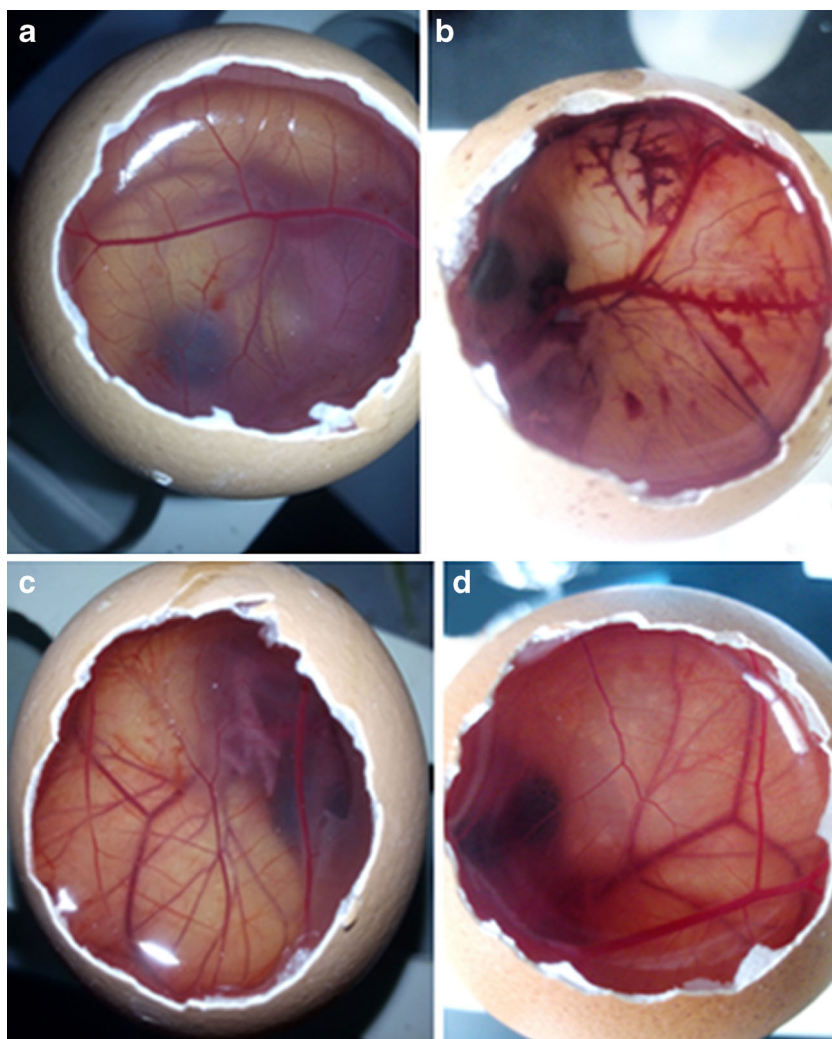


Fig. 7. Hen's egg chorioallantoic membrane treated with formulations. **a** TM-GC-NP solution. **b** 0.1 M NaOH. **c** TM-CS-NP solution. **d** 0.9% NaCl

Apparent Oil–Water Partition Coefficient

The apparent oil–water partition coefficient is an important indicator of lipophilicity of a drug, which can predict the degree of drug distribution balance between water and a biofilm (40). The corneal epithelium is the rate-limiting barrier for transcorneal diffusion of hydrophilic drugs whereas the stroma is a diffusional barrier to highly lipophilic drugs (22). Consequently, adequate solubility in both epithelium and stroma is required for effective corneal permeation. TM is hydrophilic and water soluble and has difficulty penetrating through the cornea. Results of apparent oil–water partition coefficient at different pH were shown in Table V. The weak alkaline drug TM gradually presented non-ionic form as the pH increased and its oil–water partition coefficient increased accordingly. The apparent oil–water partition coefficient of the NPs also increased with increasing of pH, and the solubility of the TM-GC-NPs in the oil phase was greater than that of TM-CS-NPs, suggesting that TM-GC-NPs may have a higher lipophilicity and consequently higher affinity for the lipophilic epithelium of the cornea. This probably could be explained by the higher pH of GC-NPs favoring

the non-ionic form of TM penetrating the cornea, which is important to predict drug absorption *in vivo* (23).

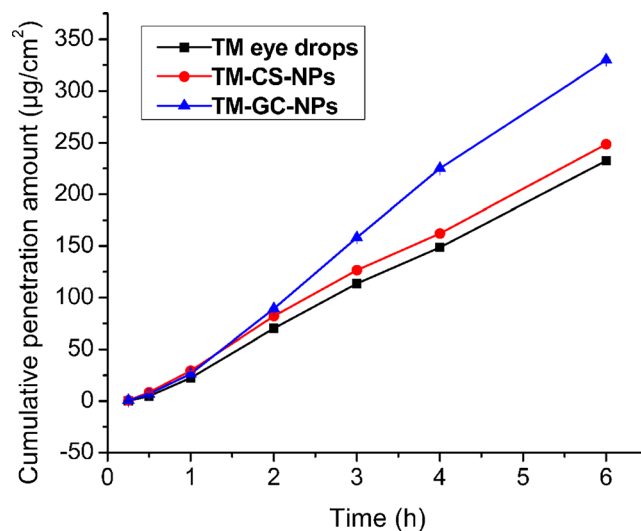


Fig. 8. Cumulative permeation profiles of commercial eye drops, TM-CS-NPs, and TM-GC-NPs ($n=3$, mean values \pm SD)

Table VII. Transcorneal Penetration Parameters of Sample *In Vitro* ($n = 6$, Mean Values \pm SD)

Sample	Commercial eye drops	TM-CS-NPs	TM-GC-NPs
$P_{app} \times 10^{-6}/(\text{cm s}^{-1})$	6.53 ± 0.13	6.92 ± 0.28	9.45 ± 0.15

TM-CS-NPs timolol-loaded chitosan nanoparticles, TM-GC-NPs timolol maleate-loaded galactosylated chitosan nanoparticles

In Vitro Release Study

Figure 6 illustrated the *in vitro* release profile of TM from different formulations over time. In the case of the TM eye drops, approximately 48 and 89% of TM was released after 0.5 and 2 h, respectively. The commercial TM eye drops showed a rapid release which was ascribed to fast diffusion of the small molecule drugs. It was observed that TM-GC-NPs and TM-CS-NPs showed initial burst release of 32 and 36% in 1 h followed by extended release of 91 and 90% in 8 h, respectively. An initial rapid release may be beneficial from a clinical perspective to achieve the therapeutic concentration of the drug in minimal time followed by sustained release of the drug to maintain a minimal effective concentration (30). The early pronounced burst release may be due to the diffuse of the drug adsorbed on the surface of NPs or weakly encapsulated into the polymeric network (39). Extended release occurring later may be explained by interaction between TM encapsulated in the NPs and the polymer, swelling, and degradation of polymer matrix.

To obtain a deeper insight into the mechanism of the drug release, the *in vitro* release data of the optimized TM-GC-NPs was fitted into different kinetic release models to select the best fitted model. It can be seen in Table VI that Ritger–Peppas model was the best fit model with $R^2 = 0.9405$ and diffusion exponent $n = 0.4841$, which indicated the release mechanism was non-Fickian transport (41). This suggested the release of drug from TM-GC-NPs was governed by erosion of polymers and diffusion from the NPs (42).

Ocular Tolerance Test (HET-CAM Test)

The HET-CAM assay is a qualitative method to assess the potential irritancy of chemicals (29). The chorioallantoic membrane of the chick embryo has complete tissues including arteries, veins, and capillaries, giving the similar result as conjunctival tissue on inflammation. Besides, the HET-CAM assay lowers test cost and prevents suffering in mammalian animals (43). The effects of control and test substances after 5 min of application on the CAM were shown in Fig. 7. The

average HET-CAM scores for 0.9% NaCl and 0.1 M NaOH solution were 0 and 11.67 ± 0.02 , respectively. The average irritation scores calculated for TM-CS-NP and TM-GC-NP solutions were 0.51 ± 0.01 and 0.27 ± 0.03 respectively, showing that the test substances were practically non-irritant. The TM-GC-NPs are likely to be well tolerated and safe for ophthalmic use.

In Vitro Transcorneal Permeation Study

The results of *in vitro* transcorneal permeation study per unit area are presented in Fig. 8. A nearly linear relationship between the cumulative amounts of penetrated drug and time was observed, indicating that the permeation rate of the formulation was steady.

As can be observed in Table VII, the corneal permeability coefficient (P_{app}) of commercial eye drops and TM-CS-NP and TM-GC-NP solutions were about $6.53 \times 10^{-6} \text{ cm s}^{-1}$, $6.92 \times 10^{-6} \text{ cm s}^{-1}$, and $9.45 \times 10^{-6} \text{ cm s}^{-1}$, respectively. When compared with commercial eye drops, the TM-GC-NPs showed a 1.45-fold increase in P_{app} , suggesting enhanced penetration achieved by TM-GC-NPs. This was most likely related to the apparently increased oil–water partition coefficient and nanosize of TM-GC-NPs. Increased lipophilicity of TM-GC-NPs with higher pH could possibly enhance corneal epithelium permeation for a hydrophilic drug as compared to TM-CS-NPs, which was consistent with the inference obtained from previous study. Furthermore, the positive charge of TM-GC-NPs might allow interaction with negatively charged mucin on the corneal surface, which could further enhance the precorneal retention of NPs compared with the commercial eye drops (12,44).

Confocal Laser Scanning Microscopy Study

The extent of transcorneal permeation of the formulations was evaluated by CLSM through florescent intensity and the depth of penetration. The corneal images obtained were shown in Figs. 9 and 10. The commercial eye drops permeated to a depth of $21.56 \pm 0.21 \mu\text{m}$ during 1 h. TM-GC-

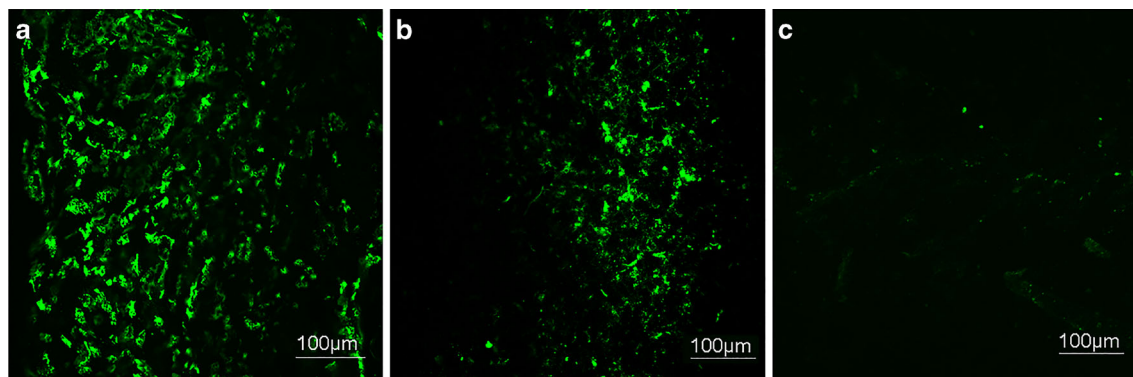


Fig. 9. CLAM micrographs of optical cornea cross-section (a TM-GC-NPs, b TM-CS-NPs, c TM eye drops)

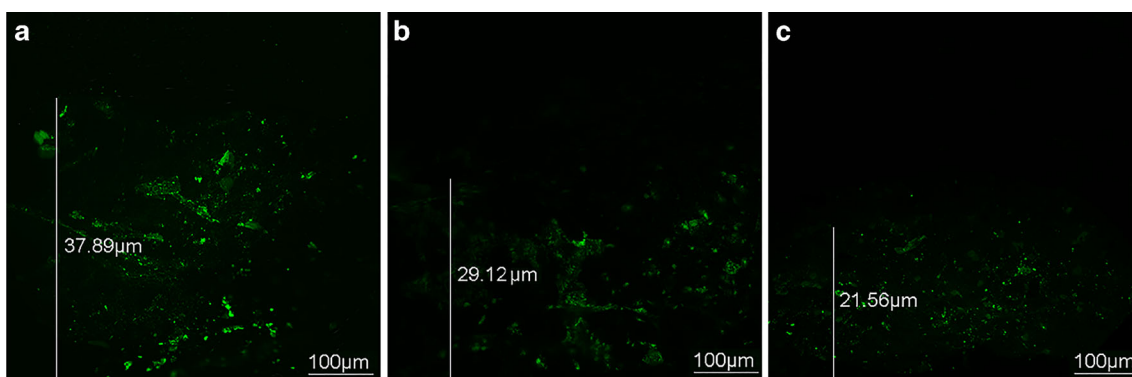


Fig. 10. CLAM micrographs of optical cornea cross-section (**a** TM-GC-NPs, **b** TM-CS-NPs, **c** TM eye drops)

NPs and TM-CS-NPs were found to penetrate the corneal epithelium up to depths of 37.89 ± 0.15 and 29.12 ± 0.18 μm , respectively, with high fluorescence intensity. The following factors may be used to illuminate this phenomenon: First, the positively charged GC-NPs interact with negatively charged sites on the cornea, which favors drug retention on the cornea. Second, TM-GC-NPs had a higher affinity for the lipophilic epithelium of the cornea and CS has the ability to open the tight junctions between epithelial cells, both of which can facilitate corneal permeation of drug jointly (9). Third, the enhanced permeability of the formulations could also be a result of its colloidal size and morphology (45).

Preocular Retention Study

In vivo imaging technology could provide high sensitivity and real-time images when the formulations loading the fluorescent dye were transported to targets (46). *In vivo* imaging of three formulations was shown in Fig. 11. The three formulations without IR783 were respectively used as control group being dropped onto the same corneas. As shown in Fig. 11a, after 1.5 h, very weak fluorescence was observed in the IR783-TM eye drops group. This

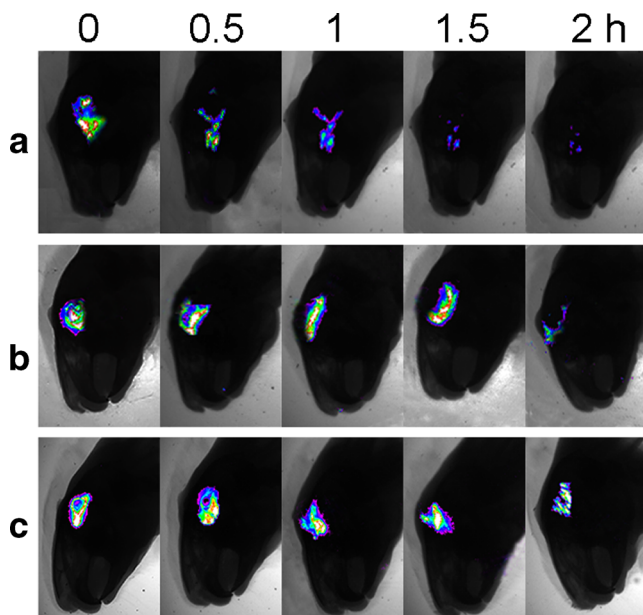


Fig. 11. *In vivo* fluorescence imaging of **a** TM eye drops, **b** TM-CS-NPs, and **c** TM-GC-NPs

may be due to the rapid corneal elimination caused by the flowability of the TM eye drops. The TM-GC-NPs show longer retention time and greater fluorescence intensity on cornea than the other two formulations. This precorneal retention could be explained by the interaction between positive charge of GC-NPs and negatively charged mucin on the corneal surface, which could further enhance the corneal permeability of NPs and bring about increased bioavailability.

Therapeutic Efficacy Study in Rabbits

The results of pharmacodynamic study were depicted as the changes of the IOP (ΔIOP) versus time in Fig. 12. The IOP-lowering activity of TM-GC-NPs reached a maximum value of 10.5 ± 0.51 mmHg within 4 h after instillation, while the peak effects of the TM-CS-NPs and commercial eye drops were 8.15 ± 0.43 mmHg at 3 h and 6.8 ± 0.35 mmHg, respectively. The commercial eye drops presented no IOP-lowering effect approximately 8 h after administration, while TM-GC-NPs and TM-CS-NPs continued to lower the IOP up to 12 h. The small change in IOP levels observed in the normal saline group may be attributed to local anesthesia of the eye. In comparison to the other two groups, TM-GC-NPs had a better therapeutic effect and a longer working time ($P \leq 0.05$) than the other two treatment groups. The prolonged

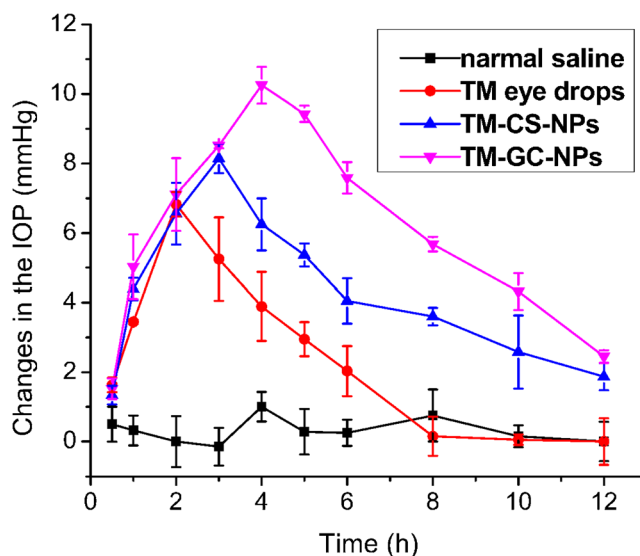


Fig. 12. Changes in the IOP as a function of time for rabbits with glaucoma ($n = 6$, mean values \pm SD)

effect of the developed formulations may be due to increased mucoadhesion of GC that interacts with negatively charged mucin effectively (47). Meanwhile, TM-GC-NPs had superior in corneal permeation and produced better efficacy in decreasing IOP. The TM-GC-NPs significantly improved drug efficacy and enhanced bioavailability.

CONCLUSION

In this study, an optimized TM-GC-NP solution was developed with an average particle size of 223.3 ± 6.83 nm, entrapment efficiency of $38.58 \pm 1.31\%$ and drug loading of $17.72 \pm 0.28\%$. The *in vitro* release study demonstrated that TM-GC-NPs had sustained release effect compared to commercial TM eye drops. The HET-CAM irritation assay confirmed that the formulation was likely to be nonirritating. The results of the transcorneal permeation study and CLSM indicated that the TM-GC-NP solution can improve drug permeability. The *in vivo* pharmacodynamic study illustrated that the formulation significantly improved the efficacy of the drug and enhanced bioavailability. On the basis of the evaluation and comparison with the commercial timolol eye drops and TM-CS-NPs, TM-GC-NP formulations are thus considered a better delivery system for the treatment of glaucoma.

ACKNOWLEDGEMENTS

The authors gratefully acknowledge the financial support from the Basic Research and Cutting-Edge Technology in Henan Province (122300410103). Moreover, we appreciate the Pharmaceutical College of Zhengzhou University for instrumental and technical support.

COMPLIANCE WITH ETHICAL STANDARDS

All studies were conducted in accordance with the Principles of Laboratory Animal Care (NIH Publication No. 92-93, revised in 1985) and were approved by the local ethics committees for animal experimentation.

Conflict of Interest The authors declare that they have no conflict of interest.

REFERENCES

- Cheng YH, Hung KH, Tsai TH, Lee CJ, Ku RY, Chiu AW, *et al.* Sustained delivery of latanoprost by thermosensitive chitosan-gelatin-based hydrogel for controlling ocular hypertension. *Acta Biomater.* 2014;10:4360-6.
- Leonardi A, Bucolo C, Drago F, Salomone S, Pignatello R. Cationic solid lipid nanoparticles enhance ocular hypotensive effect of melatonin in rabbit. *Int J Pharm.* 2015;478:180-6.
- Kim H-J, Zhang K, Moore L, Ho D. Diamond nanogel-embedded contact lenses mediate lysozyme-dependent therapeutic release. *ACS Nano.* 2014;8:2998-3005.
- Mealy JE, Fedorchak MV, Little SR. In vitro characterization of a controlled-release ocular insert for delivery of brimonidine tartrate. *Acta Biomater.* 2014;10:87-93.
- Musumeci T, Bucolo C, Carbone C, Pignatello R, Drago F, Puglisi G. Polymeric nanoparticles augment the ocular hypotensive effect of melatonin in rabbits. *Int J Pharm.* 2013;440:135-40.
- Jung HJ, Abou-Jaoude M, Carbia BE, Plummer C, Chauhan A. Glaucoma therapy by extended release of timolol from nanoparticle loaded silicone-hydrogel contact lenses. *J Control Release.* 2013;165:82-9.
- Yu S, Wang QM, Wang X, Liu D, Zhang W, Ye T, *et al.* Liposome incorporated ion sensitive in situ gels for ophthalmic delivery of timolol maleate. *Int J Pharm.* 2015;480:128-36.
- Kiland JA, Gabelt BT, Kaufman PL. Studies on the mechanism of action of timolol and on the effects of suppression and redirection of aqueous flow on outflow facility. *Exp Eye Res.* 2004;78:639-51.
- Almeida H, Amaral MH, Lobao P, Lobo JM. In situ gelling systems: a strategy to improve the bioavailability of ophthalmic pharmaceutical formulations. *Drug Discov Today.* 2014;19:400-12.
- Wu Y, Yao J, Zhou J, Dahmani FZ. Enhanced and sustained topical ocular delivery of cyclosporine A in thermosensitive hyaluronic acid-based in situ forming microgels. *Int J Nanomed.* 2013;8:3587-601.
- Tran TH, Nguyen TD, Poudel BK, Nguyen HT, Kim JO, Yong CS, *et al.* Development and evaluation of artesunate-loaded chitosan-coated lipid nanocapsule as a potential drug delivery system against breast cancer. *AAPS PharmSciTech.* 2015;16:1307-16.
- Gallarate M, Chirio D, Bussano R, Peira E, Battaglia L, Baratta F, *et al.* Development of O/W nanoemulsions for ophthalmic administration of timolol. *Int J Pharm.* 2013;440:126-34.
- Ciolino JB, Stefanescu CF, Ross AE, Salvador-Culla B, Cortez P, Ford EM, *et al.* In vivo performance of a drug-eluting contact lens to treat glaucoma for a month. *Biomaterials.* 2014;35:432-9.
- Rho S, Park I, Seong GJ, Lee N, Lee C-K, Hong S, *et al.* Chronic ocular hypertensive rat model using microbead injection: comparison of polyurethane, polymethylmethacrylate, silica and polystyrene microbeads. *Curr Eye Res.* 2014;39:917-27.
- Shukla SK, Mishra AK, Arotiba OA, Mamba BB. Chitosan-based nanomaterials: a state-of-the-art review. *Int J Biol Macromol.* 2013;59:46-58.
- Cheng YH, Tsai TH, Jhan YY, Chiu AW, Tsai KL, Chien CS, *et al.* Thermosensitive chitosan-based hydrogel as a topical ocular drug delivery system of latanoprost for glaucoma treatment. *Carbohydr Polym.* 2016;144:390-9.
- Li J, Liu H, Liu LL, Cai CN, Xin HX, Liu W. Design and evaluation of a brinzolamide drug-resin in situ thermosensitive gelling system for sustained ophthalmic drug delivery. *Chem Pharm Bull.* 2014;62:1000-8.
- Tayel SA, El-Nabarawi MA, Tadros MI, Abd-Elsalam WH. Positively charged polymeric nanoparticle reservoirs of terbinafine hydrochloride: preclinical implications for controlled drug delivery in the aqueous humor of rabbits. *AAPS PharmSciTech.* 2013;14:782-93.
- Cho IS, Park CG, Huh BK, Cho MO, Khatun Z, Li Z, *et al.* Thermosensitive hexanoyl glycol chitosan-based ocular delivery system for glaucoma therapy. *Acta Biomater.* 2016;39:124-32.
- Song B, Zhang W, Peng R, Huang J, Me T, Li Y, *et al.* Synthesis and cell activity of novel galactosylated chitosan as a gene carrier. *Colloid Surf B.* 2009;70:181-6.
- Elbially NS, Abdol-Azim BM, Shafaa MW, El Shazly LH, El Shazly AH, Khalil WA. Enhancement of the ocular therapeutic effect of prednisolone acetate by liposomal entrapment. *J Biomed Nanotechnol.* 2013;9:2105-16.
- Bucolo C, Drago F, Salomone S. Ocular drug delivery: a clue from nanotechnology. *Front Pharmacol.* 2012;3:1-3.
- Suhonen P, Jarvinen T, Koivisto S, Urtti A. Different effects of pH on the permeation of pilocarpine and pilocarpine prodrugs across the isolated rabbit cornea. *Eur J Pharm Sci.* 1998;6:169-76.
- Katiyar S, Pandit J, Mondal RS, Mishra AK, Chuttani K, Aqil M, *et al.* In situ gelling dorzolamide loaded chitosan nanoparticles for the treatment of glaucoma. *Carbohydr Polym.* 2014;102:117-24.
- Lou J, Hu W, Tian R, Zhang H, Jia Y, Zhang J, *et al.* Optimization and evaluation of a thermoresponsive ophthalmic in situ gel containing curcumin-loaded albumin nanoparticles. *Int J Nanomed.* 2014;9:2517-25.

26. Hermans K, Van den Plas D, Everaert A, Weyenberg W, Ludwig A. Full factorial design, physicochemical characterisation and biological assessment of cyclosporine A loaded cationic nanoparticles. *Eur J Pharm Biopharm.* 2012;82:27–35.
27. Zhang W, Li X, Ye T, Chen F, Yu S, Chen J, *et al.* Nanostructured lipid carrier surface modified with Eudragit RS 100 and its potential ophthalmic functions. *Int J Nanomed.* 2014;9:4305–15.
28. Katara R, Majumdar DK. Eudragit RL 100-based nanoparticulate system of aceclofenac for ocular delivery. *Colloid Surf B.* 2013;103:455–62.
29. Hao J, Wang X, Bi Y, Teng Y, Wang J, Li F, *et al.* Fabrication of a composite system combining solid lipid nanoparticles and thermosensitive hydrogel for challenging ophthalmic drug delivery. *Colloid Surf B.* 2014;114:111–20.
30. Shi S, Zhang Z, Luo Z, Yu J, Liang R, Li X, *et al.* Chitosan grafted methoxy poly(ethylene glycol)-poly(epsilon-caprolactone) nanosuspension for ocular delivery of hydrophobic diclofenac. *Sci Rep.* 2015;5:1–12.
31. Mishra V, Jain NK. Acetazolamide encapsulated dendritic nanoarchitectures for effective glaucoma management in rabbits. *Int J Pharm.* 2014;461:380–90.
32. Moya-Ortega MD, Alves TF, Alvarez-Lorenzo C, Concheiro A, Stefansson E, Thorsteinsdottir M, *et al.* Dexamethasone eye drops containing gamma-cyclodextrin-based nanogels. *Int J Pharm.* 2013;441:507–15.
33. Dai Y, Zhou R, Liu L, Lu Y, Qi J, Wu W. Liposomes containing bile salts as novel ocular delivery systems for tacrolimus (FK506): in vitro characterization and improved corneal permeation. *Int J Nanomed.* 2013;8:1921–33.
34. Liu R, Wang S, Fang S, Wang J, Chen J, Huang X, *et al.* Liquid crystalline nanoparticles as an ophthalmic delivery system for tetrandrine: development, characterization, and in vitro and in vivo evaluation. *Nanoscale Res Lett.* 2016;11:254.
35. Kim H-G, Park J-W, Park S-W. Experimental chronic ocular hypertension by anterior chamber injection of 0.3% carbomer solution in the rat. *Clin Exp Ophthalmol.* 2013;41:404–12.
36. Singh KH, Shinde UA. Chitosan nanoparticles for controlled delivery of brimonidine tartrate to the ocular membrane. *Pharmazie.* 2011;66:594–9.
37. Li XY, Li LL, Zhang ZL, Chen H. An overview on pharmacokinetics, disposition, and safety of nanoparticles in ocular applications. *Curr Drug Metab.* 2013;14:857–62.
38. Li J, Wu L, Wu W, Wang B, Wang Z, Xin H, *et al.* A potential carrier based on liquid crystal nanoparticles for ophthalmic delivery of pilocarpine nitrate. *Int J Pharm.* 2013;455:75–84.
39. Abrego G, Alvarado HL, Egea MA, Gonzalez-Mira E, Calpena AC, Garcia ML. Design of nanosuspensions and freeze-dried PLGA nanoparticles as a novel approach for ophthalmic delivery of pranoprofen. *J Pharm Sci.* 2014;103:3153–64.
40. Loftsson T, Jansook P, Stefansson E. Topical drug delivery to the eye: dorzolamide. *Acta Ophthalmol.* 2012;90:603–8.
41. Vasi AM, Popa MI, Tanase EC, Butnaru M, Verestiuc L. Poly(acrylic acid)-poly(ethylene glycol) nanoparticles designed for ophthalmic drug delivery. *J Pharm Sci.* 2014;103:676–86.
42. Ibrahim MM, Abd-Elgawad AE, Soliman OA, Jablonski MM. Nanoparticle-based topical ophthalmic formulations for sustained celecoxib release. *J Pharm Sci.* 2013;102:1036–53.
43. Elkasabgy NA. Ocular supersaturated self-nanoemulsifying drug delivery systems (S-SNEDDS) to enhance econazole nitrate bioavailability. *Int J Pharm.* 2014;460:33–44.
44. Abdullah TA, Ibrahim NJ, Warsi MH. Chondroitin sulfate-chitosan nanoparticles for ocular delivery of bromfenac sodium: improved permeation, retention, and penetration. *Int J Pharm Investig.* 2016;6:96–105.
45. Swaminathan S, Vavia PR, Trotta F, Cavalli R. Nanosponges encapsulating dexamethasone for ocular delivery: formulation design, physicochemical characterization, safety and corneal permeability assessment. *J Biomed Nanotechnol.* 2013;9:998–1007.
46. Ye T, Zhang W, Sun M, Yang R, Song S, Mao Y, *et al.* Study on intralymphatic-targeted hyaluronic acid-modified nanoliposome: influence of formulation factors on the lymphatic targeting. *Int J Pharm.* 2014;471:245–57.
47. Rekha MR, Sharma CP. Simultaneous effect of thiolation and carboxylation of chitosan particles towards mucoadhesive oral insulin delivery applications: an in vitro and in vivo evaluation. *J Biomed Nanotechnol.* 2015;11:165–76.